ANALYSIS OF FLUORESCENCE DECAY KINETICS FROM VARIABLE-FREQUENCY PHASE SHIFT AND MODULATION DATA

JOSEPH R. LAKOWICZ, GABOR LACZKO, AND HENRYK CHEREK
Department of Biological Chemistry, University of Maryland, School of Medicine, Baltimore, Maryland 21201

ENRICO GRATTON AND MARK LIMKEMAN
Department of Physics, University of Illinois at Urbana-Champaign, Urbana, Illinois 61801

ABSTRACT Recently it has become possible to measure fluorescence phase-shift and modulation data over a wide range of modulation frequencies. In this paper we describe the analysis of these data by the method of nonlinear least squares to determine the values of the lifetimes and fractional intensities for a mixture of exponentially decaying fluorophores. Analyzing simulated data allowed us to determine those experimental factors that are most critical for successfully resolving the emissions from mixtures of fluorophores. The most critical factors are the accuracy of the experimental data, the relative difference of the individual decay times, and the inclusion of data measured at multiple emission wavelengths. After measuring at eight widely spaced modulation frequencies, additional measurements yielded only a modest increase in resolution. In particular, the uncertainty in the parameters decreased approximately as the reciprocal of the square root of the number of modulation frequencies. Our simulations showed that with presently available precision and data for one emission bandpass, two decay times could be accurately determined if their ratio were ≥ 1.4. Three exponential decays could also be resolved, but only if the range of the lifetimes were fivefold or greater. To reliably determine closely-spaced decay times, the data were measured at multiple emission wavelengths so that the fractional intensities of the components could be varied. Also, independent knowledge of any of the parameters substantially increased the accuracy with which the remaining parameters could be determined. In the subsequent paper we present experimental results that broadly confirm the predicted resolving potential of variable-frequency phase-modulation fluorometry.

INTRODUCTION

During the past decade, time-resolved fluorescence measurements have become widely used in biochemical and chemical research (1, 2). Examples include resolution of the emission from mixtures of fluorophores (3–5), analysis of excited-state reactions (6–9), excited-state energy transfer (10–11), and determination of time-resolved emission spectra (12–13). Such measurements have been performed using both small molecules and more complex samples consisting of proteins and/or membranes (14–17). Time-resolved data are most often obtained using pulsed excitation, and then the time-dependent decays of fluorescence intensity are measured. By iterative reconvolution, one estimates the impulse-response function of the sample, that is, the decay of intensity that would be observed for delta-function excitation. The impulse-response function, $I(t)$, is then interpreted by comparing it with predictions from various assumed models.

An alternative to the pulse method is the technique of phase-modulation fluorometry (18–21). Instead of a pulsed excitation, the excitation beam is intensity modulated sinusoidally at a frequency comparable to the decay rates of the sample. Information concerning the decay law of the sample is obtained from the phase shift (ϕ) and the modulation (m) of the emission, both measured relative to the phase and modulation of the incident light. Under ideal experimental circumstances, it is generally accepted that both pulse and phase-modulation techniques yield equivalent information. For pulse fluorometry, it is ideal to have a narrow excitation pulse. For phase-modulation fluorometry, it is ideal to have a wide range of modulation frequencies. Developments in laser technology have made progressively shorter pulses of light available and, hence, have stimulated growth in the field of pulse fluorometry (22–23). In contrast, most available phase-modulation fluorometers operate at only two or three modulation frequencies, which greatly limits the information content and/or resolv-

G. Laczko is on leave from Jozef Atilla University, Szeged, Hungary and H. Cherek is on leave from Nicholas Copernicus University, Torun, Poland.

ing power of the measurements. Consequently, a great deal of effort has gone into extending the usefulness of the one- or two-frequency data. Specifically, Weber developed a mathematical solution whereby these data can be used to solve for the lifetimes and fractional amplitudes in a multiexponential decay (24). An alternative experimental procedure for resolving such complex decays, based on phase-sensitive detection of fluorescence, was developed by Lakowicz and co-workers (25–26).

It is apparent from recent results in at least two laboratories (27–29) that phase-modulation fluorometers, which operate over a range of modulation frequencies, are feasible and are likely to become widely available. Historically, the limiting factor has been the Debye Sears acousto-optic modulators. These modulators operate only at a few frequencies, are moderately unstable, and do not generally work at modulation frequencies >30 MHz. At present, several suitable broadband modulators are available, including electro-optic, traveling-wave electro-optic, and acousto-optic modulators (30–31). Available modulation frequencies can now range from DC to ≥300 MHz and, potentially, to ≥1 GHz. Furthermore, future developments may circumvent the limitations of these modulators. Specifically, the harmonic content of pulsed excitation sources can also be used to obtain phase and modulation data over a range of modulation frequencies (32). As a result of these recent technical accomplishments, it is now necessary to consider methods to analyze the variable-frequency data. In this paper we describe the analysis of such data by the method of nonlinear least squares (33–35), in a manner analogous to the least-squares analysis of time-correlated, photon-counting data. In our analysis we fitted the measured phase and modulation data in the frequency domain with values predicted by an assumed model, which was also calculated in the frequency domain. This method is distinct from those described previously (24–26, 36) in that the system can be over-determined by using many modulation frequencies and the analysis is not limited to a double-exponential decay. Our simulations and analysis illustrate for the first time the resolving power of the variable-frequency measurements with currently attainable accuracy. In the subsequent paper (29), we describe experimental data that demonstrate that the predicted resolution can be experimentally realized.

THEORY

The objective of the fitting procedure is twofold. First, we wish to test the validity of an assumed model. For instance, we may wish to test whether the decay is a single, double, or triple exponential. Also, one wishes to determine the parameters associated with the model and the uncertainties associated with the parameters.

The fitting routine finds the best possible match between the measured phase (ϕ_ω) and modulation (m_ω) values with those predicted on the basis of an assumed decay law ($\phi_{c\omega}$ and $m_{c\omega}$). The subscript ω is an index of the modulation frequency ($\omega = 2\pi \cdot$ frequency) and the subscript c indicates calculated values. We assume that the impulse response function $I(t)$, at any time t, can be represented by a sum of n exponential decays,

$$I(t) = \sum_{i=1}^{n} \alpha_i e^{-t/\tau_i}. \tag{1}$$

For a mixture of noninteracting fluorophores the values of τ_i represent the individual lifetimes and the values of α_i, the preexponential factors. The fractional steady state intensity, f_i, of each component in the mixture is given by

$$f_i = \frac{\alpha_i \tau_i}{\sum_j \alpha_j \tau_j}. \tag{2}$$

The interpretation of these parameters is more complex in the case of time-dependent solvent relaxation or other excited-state processes (2, 7). The response functions may still be represented by Eq. 1, except that the values of α_i and τ_i may not have physical significance.

Conveniently, one may predict the frequency-dependent values of ϕ and m for any assumed decay law (37–38). These values may be obtained from the sine, N_ω, and cosine, D_ω, transforms of the impulse response function,

$$N_\omega = \frac{\int_0^\infty I(t) \sin \omega t \, dt}{\int_0^\infty I(t) \, dt} \tag{3}$$

$$D_\omega = \frac{\int_0^\infty I(t) \cos \omega t \, dt}{\int_0^\infty I(t) \, dt}, \tag{4}$$

where the subscript ω indicates the frequency ω. For a multiexponential decay these transforms are

$$N_\omega \cdot J = \sum_{i=1}^{n} \frac{\alpha_i \omega \tau_i^2}{(1 + \omega^2 \tau_i^2)} \tag{5}$$

$$D_\omega \cdot J = \sum_{i=1}^{n} \frac{\alpha_i \tau_i}{(1 + \omega^2 \tau_i^2)}, \tag{6}$$

where $J = \Sigma_i \alpha_i \tau_i$. The phase and modulation values can be calculated from N_ω and D_ω and are given by

$$\phi_{c\omega} = \arctan (N_\omega / D_\omega) \tag{7}$$

$$m_{c\omega} = (N_\omega^2 + D_\omega^2)^{1/2}. \tag{8}$$

For a given sample the estimated values of α_i and τ_i are those that minimize χ^2, which is the error-weighted sum of the squared deviations between the measured and calculated values. When both phase and modulation data are available, χ^2 is given by

$$\chi^2 = \sum_\omega \frac{1}{\sigma_{\phi\omega}^2} (\phi_\omega - \phi_{c\omega})^2 + \sum_\omega \frac{1}{\sigma_{m\omega}^2} (m_\omega - m_{c\omega})^2, \tag{9}$$

where $\sigma_{\phi\omega}$ and $\sigma_{m\omega}$ are the estimated uncertainties in the phase and modulation data at each frequency, respectively. The choice of errors is discussed later. Minimization of χ^2 with respect to the parameters α_i and τ_i is a complex but thoroughly studied problem. We used the Marquardt algorithm (34) as described by Bevington (33). The detailed equations are given in the Appendix.

To facilitate interpretation of our simulations, it is useful to review the properties of a good fit between the experimental and the calculated data.

This is usually judged by the value of the reduced χ^2,

$$\chi^2_R = \frac{1}{2N - p}\chi^2 = \frac{\chi^2}{\nu}. \quad (10)$$

The term, $\nu = 2N - p$, is the number of degrees of freedom, where N is the number of frequencies for which both phase and modulation data were measured and p is the number of floating parameters. For example, if measurements are made at 16 frequencies and the data are fit to a two-component decay, then $\nu = 2(16) - 3 = 29$; one α_i value can always be fixed without loss of generality.

For the correct model and random experimental errors the value of χ^2_R is expected to fluctuate near unity. Notice that the calculated value of χ^2_R depends on the estimated errors ($\sigma_{\phi\omega}$ and $\sigma_{m\omega}$). In contrast to the photon-counting experiments (39), these errors are not estimated directly from Poisson counting statistics. For our simulated data, the errors are known because they were incorporated into the calculated values. For experimental data, they were estimated from the deviations between the measured and calculated values for known single- or multi-component solutions (29). In phase fluorometry, the meaningful errors appear to be day-to-day fluctuations in the measured quantities, rather than statistical fluctuations of these quantities during any single measurement session. This important aspect of the analysis is discussed in the subsequent paper (29).

The least-squares procedure allows estimation of the uncertainties in the parameters. One meaning of these uncertainties is as follows. If a single parameter is held fixed, not at the calculated value but rather one standard deviation away from this value, then χ^2 will increase to $\chi^2 + 1$ after all the other parameters have been optimized. We confirmed this relationship in a number of our simulations. Additionally, the dependence of χ^2 on the values of the parameters intuitively reveals the uncertainties in these values. For example, if χ^2 varies only slightly for widely different values of a parameter, then clearly the value of this parameter is uncertain. This occurs for closely spaced lifetimes, or for high degrees of correlation between the parameters. The minimum value of χ^2_R is used as a measure of the probability that the experimental data are described by the assumed model. Values of χ^2_R that are significantly greater than unity indicate that the assumed model is probably inadequate to explain the data, or suggest that systematic errors are present.

The estimated uncertainties in the derived parameters are given by the square root of the diagonal elements of the error matrix (covariance matrix, Eq. A13). The correlation coefficients between the parameters can be obtained from the off-diagonal terms. If the parameters are correlated, then the diagonal elements will not provide a good estimate for the joint confidence region of the parameters. Remember that in the present analysis the terms in the error matrix are independent of the actual experimental data. Rather, they depend on the day-to-day random errors in the measurements ($\sigma_{\phi\omega}$ and $\sigma_{m\omega}$), the frequencies used, and the parameters themselves (α_i and τ_i) (see Eqs. A8–A10). In our analysis of simulated data, we used the assumed level of random error as the values of $\sigma_{\phi\omega}$ and $\sigma_{m\omega}$.

Analysis of Phase and Modulation Data Measured at Multiple Emission Wavelengths

The equations described above are appropriate for phase and modulation values measured at a single emission wavelength or with a single emission bandpass. Because measurement of the phase and modulation data is quite rapid, one is naturally inclined to measure these data at several emission wavelengths. Such additional measurements do not substantially increase the time needed to complete the experiment. The additional data enhance the ability to resolve closely spaced lifetimes.

Analysis of the multiple-wavelength data is a straightforward extension of the procedure described above for a single emission bandpass. For a mixture of fluorophores, in which each fluorophore displays a single lifetime independent of emission wavelength, the decay law at any wavelength λ is given by

$$I(\lambda,t) = \sum_{i=1}^{n}\alpha_i(\lambda)\, e^{-t/\tau_i}. \quad (11)$$

The preexponential factors depend on emission wavelength. The fractional steady state intensity at each wavelength is given by

$$f_i(\lambda) = \frac{\alpha_i(\lambda)\tau_i}{\sum_j \alpha_j(\lambda)\tau_j}. \quad (12)$$

The sine and cosine transforms are given by expressions comparable to Eqs. 3–6, except α_i is replaced by $\alpha_i(\lambda)$. The calculated phase and modulation values also depend on emission wavelength, i.e., $\phi_{c\omega}(\lambda)$ and $m_{c\omega}(\lambda)$. The value of χ^2 is given by

$$\chi^2 = \sum_\lambda \sum_\omega \frac{1}{\sigma^2_{\phi\omega}}[\phi_\omega(\lambda) - \phi_{c\omega}(\lambda)]^2 + \sum_\lambda \sum_\omega \frac{1}{\sigma^2_{m\omega}}[m_\omega(\lambda) - m_{c\omega}(\lambda)]^2, \quad (13)$$

where $\phi_\omega(\lambda)$ and $m_\omega(\lambda)$ are the measured values at the indicated wavelengths. The detailed equations are once again given in the Appendix. Using this procedure, the values of $\alpha_i(\lambda)$ and τ_i are varied until the minimum value of χ^2 is obtained. Notice that the τ_i values are forced to be the same at all emission wavelengths, but that the $\alpha_i(\lambda)$ values are wavelength dependent. This model is appropriate for systems in which the

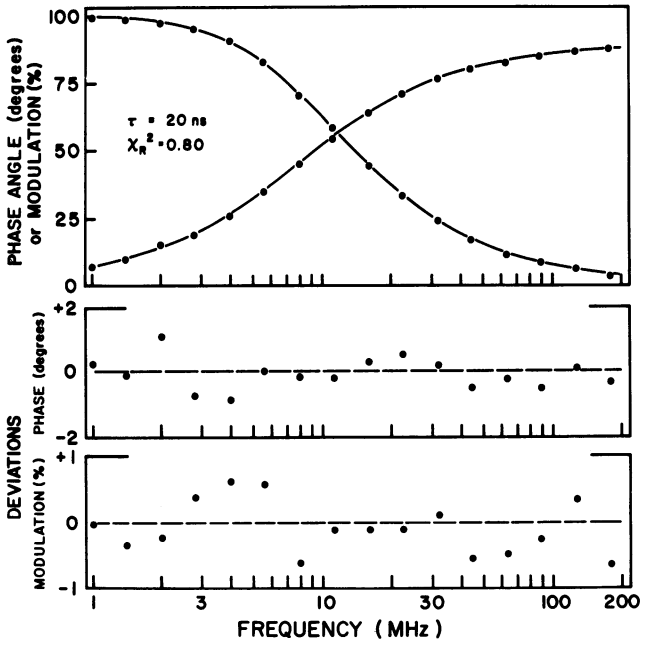

FIGURE 1 Simulated phase and modulation data for a single exponential decay are shown. The assumed decay time for the simulated data was 20 ns. Gaussian noise was added to both the phase and modulation values. For phase the added noise level (σ_ϕ) was 0.5° and for modulation the added noise (σ_m) was 0.005. The upper panel shows the simulated phase and modulation values at 16 frequencies (•). The solid line (—) is the theoretical curve for the best fit through these data. The lower panels show the deviations between the simulated and calculated values of the phase and the modulation.

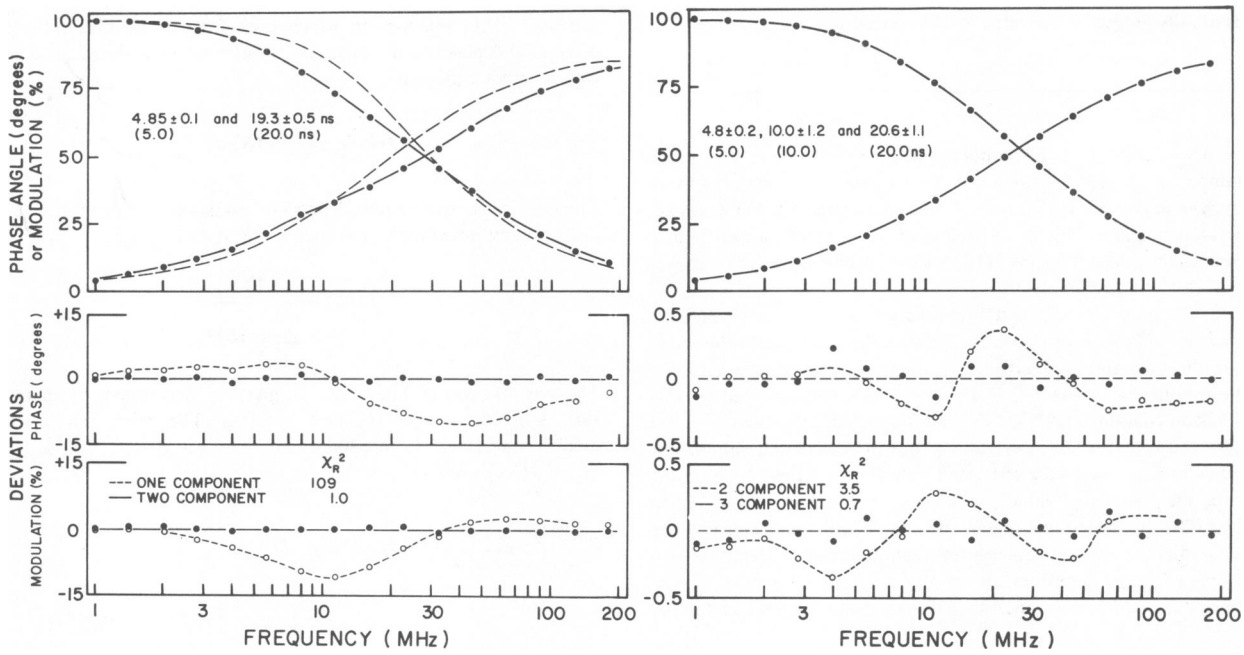

FIGURE 2 Simulated phase and modulation data for a multiexponential decays are shown. *Left*: The assumed decay times were 5 and 20 ns. The fractional intensities of the components were assumed to be equal ($f_1 = f_2 = 0.5$). The levels of added Gaussian noise were $\sigma_\phi = 0.5°$ and $\sigma_m = 0.005$. The dashed line (upper panel) and open circles (lower panels) indicate the best fit obtained using a single decay time. The solid lines and symbols represent the best fit using two decay times. *Right*: The assumed decay times were 5, 10, and 20 ns. The fractional intensities of the components were assumed to be equal ($f_1 = f_2 = f_3 = 1/3$). Gaussian noise was added at a level of 0.1% ($\sigma_\phi = 0.1°$ and $\sigma_m = 0.001$). The dashed lines and open symbols represent the best fit obtained using a two-component decay. The solid lines and symbols represent the best fit obtained using a three-component decay.

lifetime of each fluorophore is independent of emission wavelength, or for the case of a two-state, excited-state reaction (6, 7). This model is not appropriate in instances where the decay times depend on emission wavelength, such as with solvent relaxation (13–15).

RESULTS

General Features of Variable-frequency Phase and Modulation Data

Frequency-domain phase and modulation data are not widely available; hence the appearance of these data are not widely appreciated. Simulated data for single- and double-exponential decays are shown in Figs. 1 and 2. We assumed the data were measured at 16 modulation frequencies, ranging from 1 to 179.2 MHz. Measurements at this number of frequencies may be accomplished in a short time (minutes), and unless an unreasonable number of frequencies are used, additional measurements do not seem to improve the resolution. The values in the frequency range are comparable to the upper limit of 140 MHz used in the actual measurements (29). Random Gaussian error was added at a level comparable to the day-to-day fluctuations found in the experimental data (29). For most simulations we assumed a constant level of random error independent of frequency, phase angle, or modulation. The average random error in the experimental data is ±0.5° in phase angle and ±0.005 in modulation. We will refer to this as a random error of 0.5% in reference to the maximum modulation of 1.0 and the maximum phase angle of 90° (nearly 100°). However, we stress that 0.5% noise does not refer to 0.5% of the measured values, but rather 0.5% of the maximum possible phase and modulation values. To reveal the effect of random error on resolution and in anticipation of greater precision from future instruments, we considered error levels ranging from 0.1 to 1.0%.

Single-exponential Decays. Simulated data for a single-exponential decay ($\tau_1 = 20$ ns) are shown in Fig. 1. Gaussian noise was added at the level of 0.5%. Also shown is the best one-component fit. The value of τ estimated from the least-squares procedure was 19.95 ns, with an uncertainty of ±0.08 ns. Also shown in Fig. 1 are the calculated values of ϕ and m, based on the best one-component fit. The deviations between the simulated and the calculated values are shown in the lower panels. These deviations appear to be randomly distributed around zero, a result considered to indicate that there is a good fit between the experimental data and the assumed model; that is, a single-exponential decay. For this particular simulated data set we found $\chi_R^2 = 0.80$. We examined nine additional simulations with $\tau_1 = 20$ ns and 0.5% random error. Five of these simulations are shown in Table I. In each case the results were comparable to those shown in Fig. 1, except for the expected variation based on the

TABLE I
SINGLE- AND DOUBLE-EXPONENTIAL FITS TO A SINGLE-EXPONENTIAL DECAY LAW*

Simulation number	Single-exponential fit		Double-exponential fit			
	τ_1	χ^2_R	τ_1	τ_2	f_1	χ^2_R
	ns		*ns*	*ns*		
1	19.91	1.30	20.04	4.09	0.98	1.26
2	20.00	0.95	19.63	12.56	1.07	0.95
3	19.97	0.84	19.99	7.47	0.99	0.90
4	20.00	0.87	18.82	23.70	0.77	0.84
5	20.06	0.73	22.16	18.92	0.37	0.76

*The assumed parameters were 20 ns and 0.5% random error.
‡f_1 is the fractional intensity of component 1, and $f_1 + f_2 = 1.0$.

random nature of the simulated data. The estimated values of τ ranged from 19.91 to 20.16 ns, in accordance with the calculated uncertainties, and χ^2_R ranged from 0.72 to 1.30. Furthermore, we fixed the value of τ, and examined $\chi^2 = \nu \chi^2_R$. As expected, χ^2 increased approximately from 30 (χ^2) to 31 ($\chi^2 + 1$) when τ was varied by one uncertainty limit (±0.10 ns).

We attempted to fit these one-component simulations using a two-component decay law. The results of five representative simulations are summarized in Table I. The use of two-components did not result in an improved fit, as indicated by the similar values of χ^2_R. There was also a strong tendency either for the two lifetimes to be the same or for the amplitude of one of the components to approach zero. Such results indicate that including an additional component in the decay law is not justified by the experimental data.

Double-exponential Decays. Simulated data for a double-exponential decay are shown in Fig. 2 (left). The assumed lifetimes were 5 and 20 ns, the fractional intensities were assumed to be equal ($f_1 = f_2 = 0.5$), and the level of random error was 0.5% (0.5° in phase and ±0.005 in modulation). In the frequency domain the effect of a multiexponential decay is to increase the frequency range over which the phase angles are substantially different from 0° or 90°, and over which the modulation is different from 1.0 and 0. For more widely spaced lifetimes, the increased frequency range is greater and individual plateaus become apparent for each lifetime. The inadequacy of the single-component fit is evident from the systematic deviations between the simulated and calculated phase and modulation values. For the double-exponential model the deviations are substantially smaller and randomly distributed around zero (lower panels). The need for at least two-components is also evident from the values of χ^2_R. For the single- and double-exponential fits the values of χ^2_R are 109 and 1.0, respectively. The use of a still more complex decay law, i.e., three-components, did not yield smaller values of χ^2_R. Also, there was a tendency for either two of the three lifetimes to be identical or for one of the amplitudes to be zero.

Triple-exponential Decays. The previous examples may be regarded as easy resolutions because there were only two lifetimes, which were widely spaced and of comparable amplitude. The resolution of the individual decay times and amplitudes becomes difficult and ambiguous when the decay is more complex than a double exponential (39). This is illustrated in Fig. 2 (right), which contains simulated data for a three-component decay. We assumed the fractional intensities of each component were equal ($f_1 = f_2 = f_3 = 1/3$) and the lifetimes were 5, 10, and 20 ns. With random errors of 0.5%, this triple-exponential decay cannot be resolved (data not shown). Hence, the random error was decreased to 0.1% (±0.1° in phase and ±0.001 in modulation). The two- and three-component fits are shown in Fig. 2. The value of χ^2_R is decreased from 3.46 to 0.73 by assuming a third-component was present. Hence, one is inclined to accept the three-component fit. However, the deviations between the measured and calculated values are rather small using

TABLE II
ANALYSIS OF SIMULATED THREE-COMPONENT DECAYS*

Simulation number	χ^2_R		τ_1‡	τ_2	τ_3	f_1	f_2
	Two-component	Three-component					
			ns	*ns*	*ns*		
1	2.61	0.60	4.3 (0.4)	7.6 (0.8)	18.8 (0.4)	0.18	0.41
2	4.65	1.06	4.7 (0.2)	9.6 (1.1)	21.1 (1.1)	0.28	0.42
3	2.30	1.15	5.1 (0.3)	10.4 (2.7)	19.9 (1.6)	0.37	0.30
4	2.97	0.69	5.1 (1.1)	11.9 (1.3)	22.5 (7.0)	0.37	0.41
5	3.56	1.50	4.7 (0.5)	8.5 (1.6)	19.6 (1.0)	0.25	0.38
Average	3.22	1.0	4.8 (0.5)	9.6 (1.5)	20.4 (2.2)	0.29	0.35

*The assumed parameters were 5, 10, and 20 ns; 0.1% random errors; $f_1 = f_2 = f_3 = 1/3$; and $f_1 + f_2 + f_3 = 1.0$.
‡The values in parentheses are the uncertainties in the lifetimes.

either the two- or three-component decay laws. Note that the simulated data have random statistical errors whose magnitudes are accurately known. This is not the case for experimental data, which may contain both random and systematic errors. Consequently, in an experimental situation it may be difficult to choose between these fits. Additional simulations using the same assumed parameters are summarized in Table II. At this degree of precision (0.1%) the χ^2_R values of the two-component fit consistently indicate that an additional-component was present. Although the simulations in Table II indicate that the three components may be resolved, the uncertainty in the individual values is substantial (~10% on the average). For example, the estimated uncertainties in the 20, 10, and 5 ns components are 2.2, 1.5, and 0.5 ns, respectively.

Remember that the fitting procedure minimizes χ^2_R, but that this minimum value depends on the estimated errors ($\sigma_{\phi\omega}$ and $\sigma_{m\omega}$). If these are estimated correctly, the χ^2_R values will be distributed randomly about unity. However, if the values are not estimated correctly, then χ^2_R can be substantially different from unity. Because the actual level of random and systematic errors may vary among experiments, χ^2_R at ~2 or 3 may or may not indicate that an additional component should be included in the decay law. As is the case with most fitting procedures, experience is required with the instrument and the analysis in order to confidently interpret the relative and absolute values of χ^2_R.

Effects of Random Errors on Distinguishing Between Two- and Three-Component Decays

Effect of the Range of Lifetimes. The ability to distinguish between complex and simple decay laws, and the ability to reliably determine the lifetimes and amplitudes, depends strongly on the random error in the data and the difference between the individual lifetimes. The use of variable-frequency data to distinguish between single- and double-exponential decays is illustrated in Fig. 3. We calculated the value of χ^2_R for one- and two-component fits to two-component data. We observed a range of 0.7–1.3 for χ^2_R in our simulations of one- and two-component systems. Choosing a conservative approach, we selected $\chi^2_R = 3$ to unequivocally suggest that an additional component is present. Note that the extent of random error may not be known in an experiment. Hence, the magnitude of the χ^2_R values may be uncertain. After some experience with a particular measurement, a smaller decrease in the relative value of χ^2_R may be regarded as significant. Using $\chi^2_R = 3$ as a cutoff and assuming the random errors are 0.5%, a double-exponential decay can be distinguished from a single-exponential decay if the decay times differ by 40%; that is, if the long component is 20 ns and the short component is ≤12 ns. For example, a single-component fit to a simulated decay with 10- and 20-ns lifetimes results in $\chi^2_R = 9.6$, clearly indicating the need for an additional component. In contrast, if the lifetimes are 15 and 20 ns, the single-component value of χ^2_R is 1.04. This is what is expected for a two-component fit to the data, and one cannot distinguish between the two models. During these simulations it became apparent that the level of random error is the most critical factor affecting the resolution. For example, if the random error could be decreased to 0.1% (0.1° in phase and 0.001 in modulation), then a double-exponential decay could be clearly identified if the lifetimes differed by only 20%, that is, if the short component were <16 ns (lower panel). For decay times of 19 and 20 ns, χ^2_R for a one-component fit is near unity. These limits are conservative estimates, based on the rejection of χ^2_R values >3. Given an appropriate range of modulation frequencies, the χ^2_R values are dependent on the ratio of the lifetimes, not on their absolute values. Hence, the same resolution is expected for shorter lifetimes. A sample with two decay times of 4 and 5 ns could be identified if the random error were ≤0.1%.

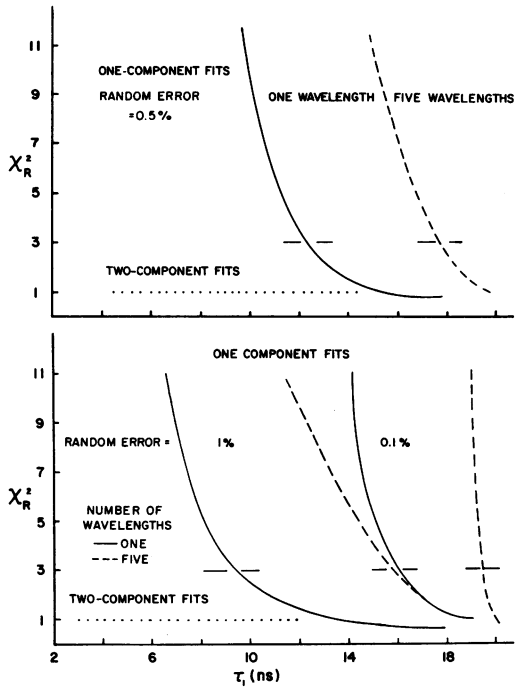

FIGURE 3 The effect of random error on the ability to distinguish between a one- or two-component decay is demonstrated. Values of χ^2_R are shown for one- and two-component fits to simulated data with two decay times. In all simulations the decay time of the long component (τ_2) was 20 ns, $f_1 = f_2 = 0.5$. The decay time of the short-component (τ_1) is indicated on the x-axis. Also shown are simulations for measurements at multiple emission wavelengths, at which the fractional intensity of each component was different. For the multiple-wavelength simulations (- - -), we assumed that measurements were performed at five emission wavelengths, such that the values of f_1 were 0.2, 0.35, 0.5, 0.65, and 0.80, and f_2 was $1 - f_1$.

Measurement at Several Emission Wavelengths. Measurements at various emission wavelengths, such that the fractional intensities of each component are varied,

makes it more easy to distinguish between one- and two-component decays. The fractional intensity of component one (f_1) was assumed to vary from 0.2 to 0.8, and f_2, from 0.8 to 0.2 (Fig. 3). We found it easier to identify a double-exponent decay by using of data measured at various emission wavelengths. For example, using the cutoff of χ^2_R = 3 and 0.5% random error, a sample containing 18- and 20-ns components could be distinguished from a single-component sample (top). With random errors of 0.1%, a two-component decay of 19.5 and 20 ns could be distinguished from a single-exponential decay (bottom). Even if the level of random error were 1%, one could still distinguish between decays of 16 and 20 ns. These results suggest that when the emission spectra of the components are different, the data should be measured at multiple emission wavelengths. The use of multiple-wavelength pulse data was described previously (40).

Three-Component Decays. We also considered the more difficult case of identifying a three-component decay from the large value of χ^2_R for the two-component fit (Fig. 4). The three lifetimes were chosen by maintaining a constant ratio between these values. We used $\tau_3/\tau_2 = \tau_2/\tau_1$, where τ_3 is the longest and τ_1 is the shortest lifetime. τ_3 was held constant and equal to 20 ns. Using χ^2_R = 3 as the cut-off and 0.5% random error, the two- and three-component fits were distinct if the intermediate lifetime were $\leq\sim$6 ns and the shortest lifetime $\leq$1.8 ns. If the precision of the measurements could be increased to 0.1%, then the two- and three-component decays could be distinguished if the shorter lifetimes were $\leq$10 and $\leq$5 ns. The increased difficulty of identifying a three-component decay is also evident from the multiple wavelength simulations. Including data at five different fractional intensities (wavelengths) narrowed the range of lifetimes needed to detect the presence of the third component, but the increase is less dramatic than that found for the two-component decays (Fig. 3).

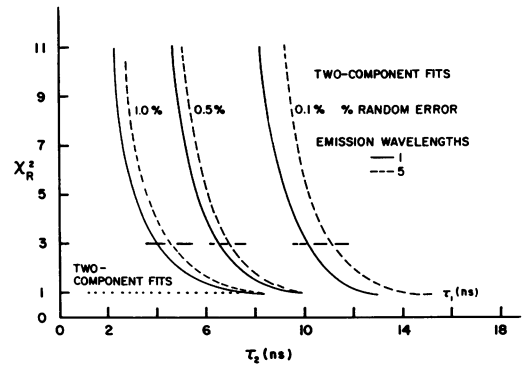

FIGURE 4 The effect of random error on the ability to distinguish between a two- and three-component decay is demonstrated. Values of χ^2_R are shown for two- and three-component fits to three-component simulations. The assumed lifetimes were selected by maintaining $\tau_3/\tau_2 = \tau_2/\tau_1$, where τ_3 and τ_1 are the longest and shortest lifetimes, respectively. τ_3 was constant and equal to 20 ns. For the multiple-wavelength simulations the fractional intensities were as follows: f_1 = 0.1, 0.2, 0.333, 0.5, 0.6; f_2 = 0.3, 0.3, 0.333, 0.3, 0.3; and τ_3 = 20 ns and f_3 = 0.6, 0.5, 0.333, 0.2, 0.1.

Accuracy in Determination of Lifetimes and Amplitudes from the Variable-frequency Data

Two-Component Decays. In the preceding section we described criteria to estimate the number of components in the decay law. We now describe how the values of the decay times and the level of random error affect the more difficult task of reliably estimating the correct decay times and fractional intensities. How well the parameters are estimated is indicated by the sensitivity of χ^2_R to variation of these same parameters. If χ^2_R depends strongly on parameter values, then these values may be determined with confidence, i.e., with low uncertainty. In contrast, if χ^2_R varies only slightly with wide variations in the parameter values, then the parameter estimates are less certain. We investigated the resolution that is possible by examining the dependence of χ^2_R on the parameter values, as suggested by Bevington (33). In particular, we fixed the parameter of interest at values bracketing the true value. Then χ^2_R was calculated by allowing the other parameters to vary so as to yield the minimum value of χ^2_R. The results of this analysis for a two-component decay with a random error of 0.1% are shown in Fig. 5 (top). The longer lifetime

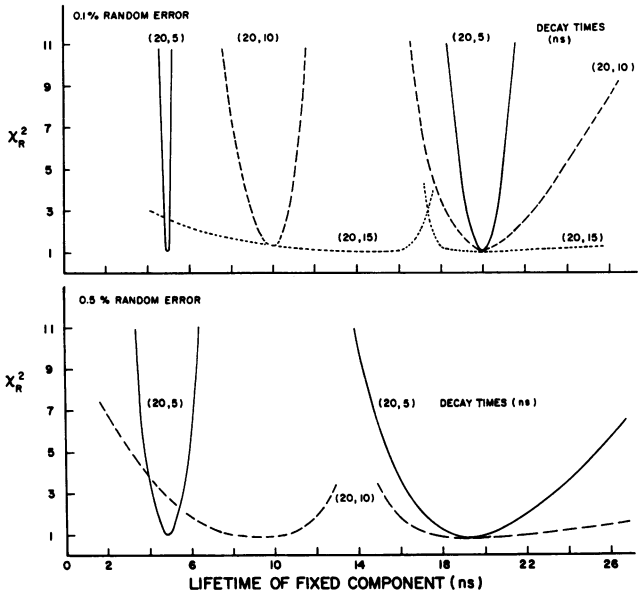

FIGURE 5 The sensitivity of χ^2_R to the values of the decay times for a two-component decay and data with random error are shown. The percentage of random error is shown in the figure. The values of χ^2_R were obtained by keeping one decay time fixed at the value indicated on the x-axis. Then, the other parameters were varied to yield a minimum value for χ^2_R. If χ^2_R increases rapidly as a lifetime is varied, then this value may be estimated with little uncertainty. If χ^2_R is not sensitive to variation of a lifetime, then the uncertainty in this estimated value is greater. In general, the lifetimes are known to be within the range where $\chi^2 = \nu\,\chi^2_R$ increases from the minimum value (χ^2_{min}) to $\chi^2_{min} + 1$.

in each simulation was 20 ns. The shorter lifetime was adjusted progressively closer to the 20-ns component. For widely spaced lifetimes (5 and 20 ns), χ^2_R is strongly dependent on both values. The minimum value of χ^2_R is sharply defined at these lifetimes. As the magnitude of the two lifetimes become comparable, χ^2_R becomes less dependent on the fixed values. For example, for data with 0.1% random error, the individual lifetimes were still determined with little uncertainty for lifetimes of 20 and 10 ns. Determination of the 20- and 15-ns decay times is less certain because χ^2_R is constant for a wide variation of the decay times. Although not shown, resolution of 18 and 20 ns appears to be impossible using data at a single-emission bandwidth, even with an uncertainty of 0.1%.

The marked effect of the random error on resolution can be seen by comparing the upper and lower panels of Fig. 5. In the lower panel the level of random error has been increased to 0.5%. The lifetimes can be resolved only if the difference is twofold, that is, 20 and 10 ns, as χ^2_R is rather insensitive to changes as large as 2 ns in the fitted lifetimes. With a random error of 0.5%, resolution of 20- and 15-ns decay times is no longer possible.

During experimentation it is frequently necessary to estimate the lifetime of a minor component in the decay. We performed simulations to indicate the lifetime uncertainty of such minor-components (Fig. 6). We used a two-component decay with decay times of 2 and 20 ns. The fractional amplitude of each-component was decreased from 50 to 10%. We chose a random error of 0.2%, which could be accomplished using the current instrument at times when its performance was better than its average performance. As the amplitude of a component decreases, χ^2_R depends less upon this component; hence the value of its decay time obtained by minimizing χ^2_R is less certain. For instance, if the fractional amplitude of the 20-ns component were 10%, then χ^2_R would change from 0.8 to 1.1 as the lifetime was changed by 2 ns. In contrast, if the fractional intensity were 50%, then a comparable change in χ^2_R would be obtained if the decay time were changed by only 0.2 ns. These results indicate that the lifetimes of components present at a level of 10% (as the steady state intensity) can be determined with currently available instrumentation if the decay times are significantly different. An increase in the noise level to 0.5% results in uncertain values for the decay time of a 10% component for the same assumed decay times.

Multiple Emission Wavelengths. We examined the effect of measurements at multiple emission wavelengths on the sensitivity of χ^2_R to the parameter values (Fig. 7). We chose a two-component decay that was barely resolvable using measurements at a single emission bandpass; where τ_1 was 15 ns, τ_2 was 20 ns, and the random error was 0.1%. The steep parabolas found for the multiple-wavelength simulation indicate that it is much easier to determine the two lifetimes. Also shown in Fig. 7 is the dependence of χ^2_R on the lifetimes when five simulations are simultaneously analyzed, but all with $f_1 = f_2 = 0.5$. These results indicate that the improved resolution provided by the multiple-wavelength measurements exceeds that obtained by repeatedly measuring the sample using the same experimental conditions.

Three-Component Decays. We also examined the sensitivity of χ^2_R to the value of each parameter used to fit a three-component decay. The value of one decay time was fixed, and we allowed the remaining parameters to vary until a minimum value of χ^2_R was obtained. We used decay times of 5, 10, and 20 ns, equal fractional intensities ($f_1 = f_2 = f_3 = 1/3$), and a random error of 0.1%. Using

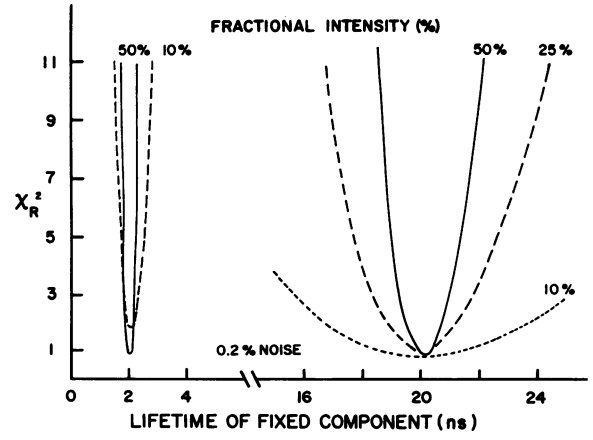

FIGURE 6 The lifetime of a small amplitude component is estimated. The assumed lifetimes in the two-component decay were 2 and 20 ns, and the added random error was 0.2%. The steady state fractional amplitude of each component is given in the figure, and the value of the fixed lifetimes is given on the x-axis. As the amplitude of a component decreases, χ^2_R becomes less sensitive to the lifetime of this component.

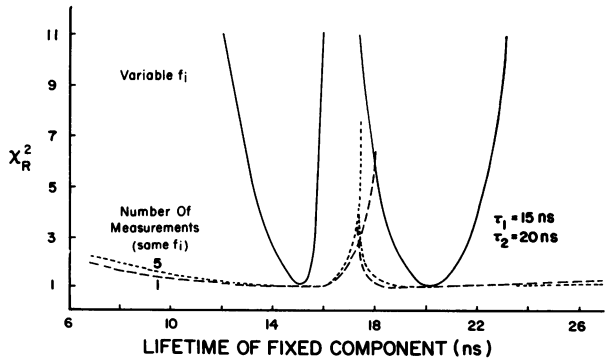

FIGURE 7 The χ^2_R values for measurements of multiple emission wavelengths (global) (—) and multiple measurements at the same emission wavelength are compared (——, - - -). The random error level was 0.1%. For the multiple measurements the fractional intensities were equal ($f_1 = f_2 = 0.5$). For the Global analysis the values of f_1 were 0.2, 0.35, 0.5, 0.65, and 0.8, and $f_2 = 1.0 - f_1$.

the results shown in Fig. 4, we concluded that this decay was more complex that a two-component decay because χ^2_R decreased from 3.2 to. 1.0 when a third component was included. Hence, it was interesting to examine the confidence with which the decay times could be determined from the fitting procedure. The results of this analysis are presented in Fig. 8. For measurements at a single emission bandwidth with no fixed parameters, χ^2_R is rather insensitive to the values of the decay times. This is especially true for the decay time of the central 10-ns component. This decay time may vary from 6 to 14 ns with a variation of χ^2_R from 1.1 at 10 ns to 1.2 at 6 and 14 ns (data not shown).

Improved resolution can be obtained by measuring the phase and modulation data at multiple emission wavelengths. We assumed that data were obtained at five emission wavelengths and that the fractional intensities of the three-components were different at each wavelength (Fig. 8). To mimic the frequent experimental situation in which all-components emit at all measurable wavelengths, the fractional intensities of each component exceeded 10% at each emission wavelength. From the results in Fig. 8, it is evident that the use of data obtained at several emission wavelengths enhances the sensitivity of χ^2_R to the values of the fitted parameters, and thus decreases the uncertainties in the parameters.

In the analysis described above, we assumed that none of the lifetimes and/or fractional intensities were known independently. In an experimental situation, one may have additional information about one or more components that may be used to improve the analysis. To model this case, we assumed that the lifetime of the central 10-ns component was known and that the data were available at a single emission bandpass. This lifetime was then fixed in the least-squares minimization (Fig. 8). This additional information substantially increased the sensitivity of χ^2_R to the values of the fitted parameters, and thereby improved the reliability of these parameters.

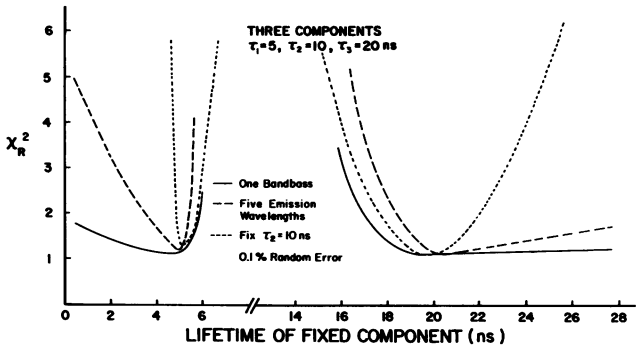

FIGURE 8 The dependence of χ^2_R on the lifetimes for a three-component decay is demonstrated. The value of χ^2_R is shown for measurements at one emission bandpass (—) and at five emission wavelengths (- - -). Also shown is a single bandpass simulation where the central lifetime (10 ns) is known (· · ·). The fractional intensities are given in Fig. 5. The random error level was 0.1%.

Sensitivity of the Parameter Estimates to Frequency Dependence in the Random Errors

In the preceding simulations we assumed that the errors had a Gaussian distribution and were independent of frequency. From our experimental work we recognized that the random errors could be dependent on the modulation frequency (29). To analyze the effect of frequency-dependent random errors, we chose multiple simulated data sets, which were derived using parameters near the limits of resolution. Specifically, we used simulated data with $\tau_1 = 10$ ns, $\tau_2 = 20$ ns, $f_1 = f_2 = 0.5$, and a random error of 0.5%. From Fig. 5 we recall that the parameters could be resolved, but that the values of χ^2_R were relatively insensitive to changes in these parameters. We reasoned that if the derived parameters were sensitive to frequency-dependent weighting of the data, this sensitivity should be most apparent for such a borderline case.

Two types of data sets were generated. The first included Gaussian errors that were independent of modulation frequency, and the second contained frequency-dependent errors comparable to those found experimentally (29). The frequency dependence of σ_ϕ was assumed to increase proportionally to log ω , from 0.1 to 1.1°, and σ_m was assumed to increase from 0.002 to 0.012 (Table III). Both types of data were analyzed with the usual frequency-independent values of σ_ϕ and σ_m, and then with frequency-dependent values ($\sigma_{\phi\omega}$ and $\sigma_{m\omega}$). The results in Table III indicate that the derived parameters are not very sensitive to the weighting factors, at least within the limited range of our simulations. We did not examine more extreme variations of $\sigma_{\phi\omega}$ and $\sigma_{m\omega}$ with frequency because such simulations would not be directly comparable with experimental data. We do not wish to diminish the importance of using the appropriate values of σ_ϕ and σ_m. Rather, we wish to indicate that the weighting factor can be estimated with sufficient accuracy from experimental data (29) and that

TABLE III
EFFECT OF DIFFERENT WEIGHTING OF THE DATA ON THE PARAMETER ESTIMATES

Frequency dependence of errors in		Averages of nine simulations		
Data	Analysis	τ_1	τ_2	f_1
		ns	*ns*	
Independent*	Independent	20.2 (1.5)§	10.0 (0.6)	0.48
Dependent‡	Independent	20.6 (2.7)	10.2 (0.9)	0.47
Independent	Dependent	21.7 (2.8)	10.2 (1.1)	0.46
Dependent	Dependent	20.9 (2.0)	10.3 (0.8)	0.45

The assumed parameters were $\tau_1 = 10$ ns, $\tau_2 = 20$ ns, $f_1 = f_2 = 0.5$, and 0.5% random error. The values shown are the average of nine independent simulations.

*Independent: $\sigma_\phi = 0.50$ and $\sigma_m = 0.005$.

‡Dependent: $\sigma_{\phi\omega} = 0.1 + 0.5 \log \omega$ and $\sigma_{m\omega} = 0.002 + 0.005 \log \omega$.

§The number in the parentheses is the average of the uncertainties.

frequency-dependent variations in σ_ϕ and σ_m will not prevent a successful analysis.

Note that, in contrast to the parameters themselves, the estimated uncertainties in the parameters are strongly dependent on the weighting factors (Eqs. A8–A12). We estimated the uncertainties from the diagonal elements of the error matrix.

Resolvability Analysis Based on the Error Matrix

Lifetime Resolution. In the preceding sections we described the ability to determine multiexponential decay parameters based on the values of χ^2_R. This is a familiar approach that is encountered in the laboratory. However, the resolvability of multiexponential decays may be described more generally. In particular, examination of the error matrix (Eqs. A8–A10) also provides an estimation of the possible resolution. The uncertainties in each parameter can be estimated using only knowledge of the errors in phase and modulation, the set of frequencies, and the dependence of ϕ and m on each parameter (Eq. A8). Inversion of the matrix yields the uncertainties in each parameter. We assume here that two lifetimes are resolvable if these values, with their associated errors, do not overlap. We stress that these estimates are based on the assumption that the linearized form of the model is valid in the region of the final estimates for the parameters.

Such calculations are presented in Fig. 9. We assumed a logarithmic, equally spaced frequency set (1, 2, 4, 8, 16, 32, 64, and 128 MHz) and an error of 0.2° and 0.004 for phase and modulation, respectively. These errors, being the same for all measurements, factor out of the error matrix. Consequently, the uncertainties in the parameters are linearly proportional to the measurement errors (Appendix). All fractional intensities were 0.5. For a given value of τ_1, it is possible to calculate the minimum and maximum values τ_2 which give nonoverlapping values of τ_1 and τ_2 considered with their associated errors. In Fig. 9 we report the minimum and maximum value of τ_2 obtained as a function of τ_1. The dashed region in this figure depicts the region where the one- and two-component decays cannot be distinguished. The resolvability plot is invariant (symmetric) for an exchange of τ_1 with τ_2, and we can define a resolvability ratio—the ratio of the maximum value of τ_2 to the value of τ_1 in the nonresolvability region. Because the width of the resolvability region in Fig. 9 is proportional to the measurement error, it is straightforward to calculate the resolvability ratio for different error values.

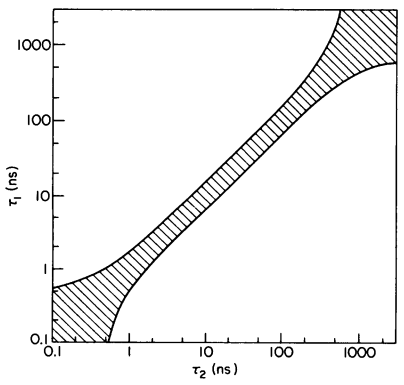

FIGURE 9 A double-exponenetial decay resolvability plot is shown. Lifetime pairs in the shaded region cannot be resolved using the frequency set 1, 2, 3, 8, 16, 32, 64, and 128 MHz if the random error of the phase and modulation measurements are 0.2° and 0.004, respectively.

There are some important points to consider in Fig. 9. First, the nonresolvability region has a width that is approximately constant from 1 to 500 ns. The position of the constant width region on the lifetime axis depends on the frequency set used. If we multiply all frequencies of the set by 2, the constant width region will move down on the lifetime axis by a factor of 2. This implies that on a log scale the resolvability plot is shape invariant. Second, for our choice of frequencies and errors, the resolvability ratio is ~1.4, which simply means that two lifetime values are resolvable if they differ by a factor of 1.4 in the region 1 to 500 ns. For example it is possible to resolve 1 and 1.4 ns, as well as 20 and 28 ns or 50 and 70 ns. Third, the width and extension of the resolvability region depends on the frequency set. Fourth, inside the resolvability region, it is impossible to distinguish between a double- and a single-exponential decay. That is, the χ^2_R obtained using a double- and single-exponential decay are too similar to determine the appropriate decay law.

Effect of Number and Choice of Modulation Frequencies. To investigate the effect of the number of frequencies on the resolvability ratio, we evaluated the error matrix as a function of the number of frequencies. In Fig. 10, we report the uncertainties of τ_1, τ_2, and f_1 as a

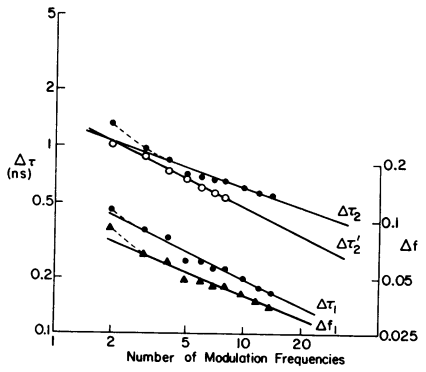

FIGURE 10 The effect of the number of frequencies on the uncertainties in the lifetimes ($\Delta\tau$) and the fractional intensities (Δf) is shown. The assumed lifetimes were τ_1 = 6.7 ns and τ_2 = 15 ns, with f_1 = 0.5. The symbols are as follows: $\Delta\tau_2$ and $\Delta\tau_1$ (●) and Δf_1 (▲) for equally spaced frequencies on the log scale from 1 to 128 MHz. The open circle indicates the uncertainty in $\Delta\tau_2'$ when two optimal frequencies are added to the total frequency set. The calculated optimum frequencies were F_1 = 10.6 MHz and F_2 = 71.3 MHz. The frequencies used were 12 and 60 MHz.

function of the number of frequencies for two selected lifetime pairs. Angular frequency values were chosen equally spaced on a log scale and symmetrically placed with respect to the reciprocals of the two lifetime values. An extensive study on a large number of lifetime pairs has shown that they have a common characteristic, an asymptotic linear behavior. In all cases investigated the slope of the linear part in Fig. 10 is between $-1/2$ and $-1/3$. This result implies that the error in the parameters decreases only as the square root or cube root of the number of frequencies. Consequently, if we want to decrease the error in the parameters by a factor of 2 (to decrease the resolvability ratio by a factor of $\sim\sqrt{2}$, we must increase the number of frequencies by a factor between 4 and 8. The errors are relatively insensitive to the number of frequencies, which imposes a practical limit on the number of frequencies to be used. The same reduction in the parameter error obtained by increasing the number of frequencies from 2 to 8 ($= 2^3$) can be obtained by increasing the number of frequencies from 8 to ~512. A set of 16 different frequencies equally spaced in a log scale in the range 1–128 MHz is adequate for most practical cases and allows for an occasional invalid measurement without complete loss of the experiment.

In the special case where a two-component decay can be quite confidently assumed, we find that an optimum two-frequency set exists for which the errors on the parameters are smaller than they are with an equivalent number of evenly spread frequencies and for which error is reduced to the greatest degree by simply averaging data at these two frequencies. Optimum two-frequency selection removes the curvature in the plots of $\Delta\tau$ vs. number of frequencies. Because the number of frequencies is increased only by averaging symmetrically at the two optimum frequencies, the error in the average value of τ will be dependent on the square root of the number of measurements. An empirical formula for finding the optimum two frequencies F_1 and F_2 is

$$F_1 = \frac{1}{2\pi\tau_2}, F_2 = \frac{3}{2\pi\tau_1}, \tag{14}$$

where $\tau_1 < \tau_2$ and, hence, $F_1 < F_2$.

Three-Component Decay. The same procedure employed to analyze the resolvability of a two-component system can be applied to the analyze a three-component system. In Fig. 11 we report the result of this analysis for a fixed value of τ_1 ($= 10$ ns) as a function of τ_2 and τ_3. This is a projection onto the τ_1, τ_2 plane of a slice (at $\tau_3 = 10$ ns) of a three-dimensional volume within which a τ_1-τ_2-τ_3 triplet cannot be resolved. For this calculation we assumed $f_1 = f_2 = f_3 = 1/3$. The frequency set and the errors were the same as those used for the analysis of a two-component system. Further analysis generally shows that a three-component system can be resolved for these frequencies and errors if the lifetimes are separated by a factor of 2.3,

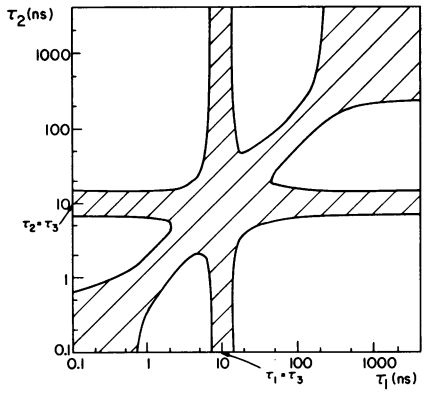

FIGURE 11 A triple-exponential decay resolvability plot, which is the same as Fig. 9 except $f_1 = f_2 = f_3 = 1/3$.

or a total range of ~fivefold. As one-component becomes further separated from the other two, those two can move closer together, and still be resolved. As with the two-component set, an optimal three-frequency set can be found for a τ_1-τ_2-τ_3 triplet. The same formula may be used for F_1 and F_2 with $\tau_1 < \tau_3 < \tau_2$. The third frequency is obtained from the first two, $F_3 = (F_1F_2)^{1/2}$.

In conclusion, analysis of the error matrix gives the general condition for resolvability of a lifetime pair or triplet. A similar analysis for different parameters values follows the same trend, but gives different resolvability ratios. As noted before, in the analysis it is important to assign experimental errors. Generally, this assignment is based on the experimental observation of the deviation around the mean of a series of identical measurements taken on a number of days, as discussed in the subsequent paper (29).

DISCUSSION

In the preceding sections we considered the use of multifrequency phase and modulation data for the resolution of multiexponential decays of fluorescence. One may question the usefulness of this method for the analysis of nonexponential decay laws. Such complex decays are observed for energy transfer (10, 11, 41), for time-dependent solvent relaxation (13, 42, 43), and for the case when substantial collisional quenching occurs when the time-dependent terms in the diffusion equations are significant (44). The analysis of such decays by phase-modulation fluorometry should pose no special problems. Basically, the impulse response function must be transformed into the frequency domain, as described by Eqs. 3 and 4. The transformations may be accomplished numerically or analytically. Then, the least-squares procedure described in Eqs. 1–9 and A1–A22 can be used. This method has already been used to calculate time-resolved emission spectra of proteins and membranes labeled with fluorescent probes (45). Similarly, differential polarized phase angles and demodulation may be used to determine the time-resolved decays of fluorescence anisotropy. Such

work is currently in progress. It appears that phase and modulation measurements, when performed over a range of modulation frequencies, will provide time-resolved data that are at least equivalent to those obtained using pulsed excitation.

APPENDIX

The minimization of χ^2 function with respect to model parameters can be accomplished using different approaches. We used the procedure described by Bevington (33, chapter 11) and Brandt (35, chapter 9). Let α_j and α_{j+1} represent the parameters α_m and τ_m for the mth exponential component of a system with n components. The maximum number of parameters is $2n$. One value of α can be fixed because either $\Sigma\, \alpha_m \tau_m$ or $\Sigma\, \alpha_m$ can be set equal to unity. For a general fit with no restricted parameters, the maximum value of j, therefore, is $2n - 1$.

The minimization procedure consists of solving the system of equations by setting to zero the derivatives of χ^2 with respect to the parameters a_j. Generally, we have a system of $2n - 1$ nonlinear equations. One usually uses a Taylor expansion of the theoretical function to linearize the function with respect to the parameters.

$$\phi_{c\omega} = \phi_{0\omega} + \sum_j \frac{\partial \phi_{0\omega}}{\partial a_j}\,\delta a_j \tag{A1}$$

$$m_{c\omega} = m_{0\omega} + \sum_j \frac{\partial m_{0\omega}}{\partial a_j}\,\delta a_j\,. \tag{A2}$$

In these expressions the zero subscript refers to the starting or current value of the parameter and the subscript ω refers to the frequency. Using these expanded functions, χ^2 is given by

$$\chi^2 = \sum_\omega \frac{1}{\sigma^2_{\phi\omega}}\left(\phi_\omega - \phi_{0\omega} - \sum_j \frac{\partial \phi_{0\omega}}{\partial a_j}\,\delta a_j\right)^2 + \sum_\omega \frac{1}{\sigma^2_{m\omega}}\left(m_\omega - m_{0\omega} - \sum_j \frac{\partial m_{0\omega}}{\partial a_j}\,\delta a_j\right)^2. \tag{A3}$$

The strategy used in the least-squares method is to calculate the parameter increments δa_j to yield the minimum value of χ^2. This occurs when all the derivatives of χ^2 with respect to the parameter increments are zero. Hence,

$$-\frac{1}{2}\frac{\partial \chi^2}{\partial \delta a_k} = \sum_\omega \frac{1}{\sigma^2_{\phi\omega}}\left(\phi_\omega - \phi_{0\omega} - \sum_j \frac{\partial \phi_{0\omega}}{\partial a_j}\,\delta a_j\right)\left(\frac{\partial \phi_{0\omega}}{\partial a_k}\right) + \sum_\omega \frac{1}{\sigma^2_{m\omega}}\left(m_\omega - m_{0\omega} - \sum_j \frac{\partial m_{0\omega}}{\partial a_j}\,\delta a_j\right)\left(\frac{\partial m_{0\omega}}{\partial a_k}\right) = 0. \tag{A4}$$

These equations can be rearranged to yield

$$\sum_\omega \frac{1}{\sigma^2_{\phi\omega}}(\phi_\omega - \phi_{0\omega})\left(\frac{\partial \phi_{0\omega}}{\partial a_k}\right) + \sum_\omega \frac{1}{\sigma^2_{m\omega}}(m_\omega - m_{0\omega})\left(\frac{\partial m_{0\omega}}{\partial a_k}\right) = \sum_\omega \frac{1}{\sigma^2_{\phi\omega}}\sum_j \left(\frac{\partial \phi_{0\omega}}{\partial a_j}\right)\left(\frac{\partial \phi_{0\omega}}{\partial a_k}\right)\delta a_j + \sum_\omega \frac{1}{\sigma^2_{m\omega}}\sum_j \left(\frac{\partial m_{0\omega}}{\partial a_j}\right)\left(\frac{\partial m_{0\omega}}{\partial a_k}\right)\delta a_j. \tag{A5}$$

This yields a set of simultaneous equations

$$\beta_k = \sum_j \alpha_{jk}\,\delta a_j, \tag{A6}$$

where

$$\beta_k = \sum_\omega \frac{1}{\sigma^2_{\phi\omega}}(\phi_\omega - \phi_{0\omega})\left(\frac{\partial \phi_{0\omega}}{\partial a_k}\right) + \sum_\omega \frac{1}{\sigma^2_{m\omega}}(m_\omega - m_{0\omega})\left(\frac{\partial m_{0\omega}}{\partial a_k}\right) \tag{A7}$$

$$\alpha_{jk} = \sum_\omega \frac{1}{\sigma^2_{\phi\omega}}\left(\frac{\partial \phi_{0\omega}}{\partial a_j}\right)\left(\frac{\partial \phi_{0\omega}}{\partial a_k}\right) + \sum_\omega \frac{1}{\sigma^2_{m\omega}}\left(\frac{\partial m_{0\omega}}{\partial a_j}\right)\left(\frac{\partial m_{0\omega}}{\partial a_k}\right). \tag{A8}$$

One can solve for the increments δa_j using the standard procedures of linear algebra. In matrix notation Eq. A6 becomes

$$\beta = \delta a \alpha, \tag{A9}$$

where β and $\delta\alpha$ are row matrices, and α is a symmetric matrix, called the curvature matrix because it describes the curvature of χ^2 in parameter space. The values of δa_j are obtained by inverting α to yield $\epsilon = \alpha^{-1}$, which is the covariance matrix of the parameters, also called the error matrix where

$$\beta\alpha^{-1} = \beta\epsilon = \delta a. \tag{A10}$$

The new value of a_j is found from $a_j = a_0 + \delta a_j$. This process is repeated using the new values of a_j until χ^2 reaches a minimum. We used the gradient-expansion algorithm in which a value λ is added to the diagonal terms of the curvature matrix. This matrix is given by

$$\alpha_{jk} = \begin{cases} \alpha_{jk} + \lambda & \text{for } j = k \\ \alpha_{jk} & \text{for } j \neq k. \end{cases} \tag{A11}$$

The value of λ is varied using the method given by Marquardt (34), as summarized by Bevington (33). Eq. A11 is different from that given in reference 33, but Eq. A11 is consistent with the description given by Marquardt (34). For small values of λ, which are used near the χ^2 minimum, the search is approximately an analytical search, assuming the Taylor expansion (Eqs. A1 and A2) is valid. For large values of λ one has

$$\beta_j = \lambda\,\delta a_j. \tag{A12}$$

Then, because β_j are the gradients of χ^2 for the jth parameter [$\beta_j = -1/2\,(\partial\chi^2/\partial a_j)$], the δa vector corresponds to the direction of the χ^2 gradient. Hence, by varying λ, one varies the estimated parameters between those suggested by the χ^2 gradients and those suggested by linearization of the function. This procedure yields rapid convergence to the minimum value of χ^2.

The uncertainties of the parameters can be estimated from the diagonal terms of the ϵ matrix (also called the covariance maxtrix). The uncertainty in a_j (σ_{a_j}) is given by

$$\sigma^2_{a_j} = \epsilon_{jj}. \tag{A13}$$

If an individual parameter a_j is held constant at $(a_j)_{\min} + \sigma_{a_j}$, and if the other parameters are varied to minimize χ^2, then χ^2 will usually increase from $\chi^2{}_{\min}$ to $\chi^2{}_{\min} + 1$. We confirmed that this was approximately true by a number of simulations. Each time the increase in χ^2 varied from 0.3 to 2.0. Of course, this is a result of the nonlinear nature of the fitting and statistical variations in the individual simulations. The off-diagonal terms of ϵ are generally nonzero, indicating that the parameters are correlated with each other. One can describe the degree of correlation between ith and jth parameters by using the correlation coefficient

$$P_{ij} = \frac{\epsilon_{ij}}{\epsilon_{ii}^{1/2}\,\epsilon_{jj}^{1/2}}\,.$$

A value of $P_{ij} = 0$ indicates no correlation, that is, the two parameters are independent. A value of j close to $+1$ or -1 indicates correlation or anticorrelation between the two parameters, which means that the two parameters can be varied accordingly without varying the χ^2 value. In this case the values of the diagonal elements (ϵ_{ii}) do not correctly estimate the uncertainties in the parameters, and the actual uncertainty will be $>\epsilon_{ii}$.

Observe that the curvature matrix α depends on the values of $\phi_{0\omega}$, $\sigma_{\phi\omega}$, $m_{0\omega}$, and $\sigma_{m\omega}$ for a given set of parameters, but is independent of the measured values ϕ_ω and m_ω (Eq. A8). If we assume frequency-independent errors σ_ϕ and σ_m and if we define $K = \sigma_m/\sigma_\phi$, where K is a constant, then the error $1/\sigma_\phi^2$ becomes a common factor for each term in the error matrix. Hence, in matrix notation we can write $\alpha = (1/\sigma_\phi^2)\,\alpha'$, where α' depends on the values of the parameters a_j and on K. The error matrix, which is the inverse of α, is $\epsilon = \sigma_\phi^2\,(\alpha')^{-1}$. The square root of the diagonal terms of the errors matrix are the uncertainties in the parameter a_j, which are proportional to σ_ϕ.

From Eqs. A7–A9, notice that solving for the parameter increments δa_j requires the partial derivatives of $\phi_{0\omega}$ and $m_{0\omega}$ with respect to the parameters. In principle one may use either numerical estimates of these derivatives or the analytical derivatives. The numerical derivatives are more sensitive to round-off errors in the computation. For our programs written in BASIC and in PASCAL we were restricted to single precision, so we used the analytical derivatives.

For convenience we redefine

$$N_\omega^* = N_\omega J \tag{A14}$$

$$D_\omega^* = D_\omega J, \tag{A15}$$

where $J = \Sigma_i\, \alpha_i\, \tau_i$. Then,

$$\frac{\partial \phi_{0\omega}}{\partial \alpha_i} = \frac{\cos^2 \phi_{0\omega}}{(D_\omega^*)^2}\left(\frac{\partial N_\omega^*}{\partial \alpha_i} D_\omega^* - N_\omega^* \frac{\partial D_\omega^*}{\partial \alpha_i}\right) \tag{A16}$$

$$\frac{\partial \phi_{0\omega}}{\partial \tau_i} = \frac{\cos^2 \phi_{0\omega}}{(D_\omega^*)^2}\left(\frac{\partial N_\omega^*}{\partial \tau_i} D_\omega^* - N_\omega^* \frac{\partial D_\omega^*}{\partial \tau_i}\right) \tag{A17}$$

$$\frac{\partial m_{0\omega}}{\partial \alpha_i} = \frac{-\tau_i m_{0\omega}}{J} + \frac{1}{J^2 m_{0\omega}}\left(N_\omega^* \frac{\partial N_\omega^*}{\partial \alpha_i} + D_\omega^* \frac{\partial D_\omega^*}{\partial \alpha_i}\right) \tag{A18}$$

$$\frac{\partial m_{0\omega}}{\partial \tau_i} = \frac{\alpha_i m_{0\omega}}{j} + \frac{1}{J^2 m_{0\omega}}\left(N_\omega^* \frac{\partial N_\omega^*}{\partial \tau_i} + D_\omega^* \frac{\partial D_\omega^*}{\partial \tau_i}\right), \tag{A19}$$

where

$$\frac{\partial N_\omega^*}{\partial \alpha_i} = \frac{\omega \tau_i^2}{1 + \omega^2 \tau_i^2} \tag{A20}$$

$$\frac{\partial D_\omega^*}{\partial \alpha_i} = \frac{\tau_i}{1 + \omega^2 \tau_i^2} \tag{A21}$$

$$\frac{\partial N_\omega^*}{\partial \tau_i} = \frac{2\,\alpha_i \omega \tau_i}{(1 + \omega^2 \tau_i^2)^2} \tag{A22}$$

$$\frac{\partial D_\omega^*}{\partial \tau_i} = \frac{\alpha_i\,(1 - \omega^2 \tau_i^2)}{(1 + \omega^2 \tau_i^2)^2}. \tag{A23}$$

Analysis of Phase and Modulation Data at Multiple Emission Wavelengths

If the phase and modulation data are measured at several emission wavelengths then somewhat more complex expressions are needed for the analysis. The sine and cosine transforms of Eq. 10 are

$$N_\omega(\lambda)\, J(\lambda) = \sum_i \frac{\alpha_i(\lambda)\, \omega \tau_i^2}{1 + \omega^2 \tau_i^2} = N_\omega^*(\lambda) \tag{A24}$$

$$D_\omega(\lambda)\, J(\lambda) = \sum_i \frac{\alpha_i(\lambda)\, \tau_i}{1 + \omega^2 \tau_i^2} = D_\omega^*(\lambda), \tag{A25}$$

where

$$J(\lambda) = \sum_j \alpha_j(\lambda) \tau_j. \tag{A26}$$

With this modification the β terms in the matrix become

$$\beta_k = \sum_\lambda \sum_\omega \frac{1}{\sigma_{\phi\omega}^2}\,[\phi_\omega(\lambda) - \phi_{0\omega}(\lambda)]\,\frac{\partial \phi_{0\omega}(\lambda)}{\partial a_k} + \sum_\lambda \sum_\omega \frac{1}{\sigma_{m\omega}^2}\,[m_\omega(\lambda) - m_{0\omega}(\lambda)]\,\frac{\partial m_{0\omega}(\lambda)}{\partial a_k}. \tag{A27}$$

Similarly, the terms in the curvature matrix become

$$\alpha_{jk} = \sum_\lambda \sum_\omega \frac{1}{\sigma_{\phi\omega}^2}\,\frac{\partial \phi_{0\omega}(\lambda)}{\partial a_j}\,\frac{\partial \phi_{0\omega}(\lambda)}{\partial a_k} + \sum_\lambda \sum_\omega \frac{1}{\sigma_{m\omega}^2}\,\frac{\partial m_{0\omega}(\lambda)}{\partial a_j}\,\frac{\partial \phi_{0\omega}(\lambda)}{\partial a_k}. \tag{A28}$$

If necessary, wavelength-dependent values of $\sigma_{\phi\omega}$ and $\sigma_{m\omega}$ could be substituted in Eqs. A27 and A28. Including data at q wavelengths increases the order of the matrix from $2n - 1$ to $2n - 1 + (q - 1)\,(n - 1)$, where n is the number of components. Recall that at each wavelength one value $\alpha_i(\lambda)$ can always be fixed, so that each additional wavelength adds $n - 1$ floating values of $\alpha_i(\lambda)$. For example, if measurements are made at 10 wavelengths ($q = 10$) and the data are fit to a three-component decay ($n = 3$), then the matrix (α) contains 23 rows and columns. In contrast, for measurements at a single wavelength the order of the matrix is five (three decay times and two values of the preexponential factors). In spite of this apparent increase in complexity, the total number of computations is simplified because a number of derivatives are equal to zero. From Eqs. A24 and A25 it is apparent that

$$\frac{\partial N_\omega^*(\lambda)}{\partial \alpha_i(\lambda')} = 0 \tag{A29}$$

$$\frac{\partial D_\omega^*(\lambda)}{\partial \alpha_i(\lambda')} = 0 \tag{A30}$$

for $\lambda \neq \lambda'$. For equal values of λ the derivatives are as follows,

$$\frac{\partial N_\omega^*(\lambda)}{\partial \alpha_i(\lambda)} = \frac{\omega \tau_i^2}{1 + \omega^2 \tau_i^2} \tag{A31}$$

$$\frac{\partial D_\omega^*(\lambda)}{\partial \alpha_i(\lambda)} = \frac{\tau_i}{1 + \omega^2 \tau_i^2} \tag{A32}$$

$$\frac{\partial N_\omega^*(\lambda)}{\partial \tau_i} = \frac{2\alpha_i(\lambda)\omega \tau_i}{(1 + \omega^2 \tau_i^2)^2} \tag{A33}$$

$$\frac{\partial D_\omega^*(\lambda)}{\partial \tau_i} = \frac{\alpha_i(\lambda)\,(1 - \omega^2 \tau_i^2)}{(1 + \omega^2 \tau_i^2)^2}. \tag{A34}$$

Programs based on the Marquadt algorithm, for both the single- and multiple-wavelength analysis were written in both BASIC and FOR-

TRAN for a Digital Minc 11/23 computer (Digital Equipment Corp., Marlboro, MA). Copies of these programs are available from J. R. Lakowicz on request. Additionally, a similar program is available in PASCAL for an Apple computer (Apple Computer Inc., Cupertino, CA). This program uses the values of δa_j to produce a new value for a_j using $a_j = a_{j0} + \delta a_j/S$, where S is a stepping factor that adjusts the rate of approach to the χ^2 minimum. The uncertainties in the parameters are estimated on the basis of the variance between the assumed model and the experimental data for a particular data set. This program also yields rapid convergence for most common experimental data, and is available on request from E. Gratton.

This work was supported by grants from the National Science Foundation: PCM 80-41320, 81-06910 and 82-10878 to J. R. Lakowicz, and PCM 79-18646 to E. Gratton. This work was performed during the tenure of an Established Investigatorship to J. R. Lakowicz from the American Heart Association.

Received for publication 21 November 1983 and in final form 29 May 1984.

REFERENCES

1. Badea, M. G., and L. Brand. 1971. Time-resolved fluorescence measurements. *Meth. Enzymol.* 61:378–425.
2. Lakowicz, J. R. 1983. Principles of Fluorescence Spectroscopy. Plenum Publishing Corp. New York. 485 pp.
3. Knutson, J. R., D. G. Walbridge, and L. Brand. 1982. Decay-associated fluorescence spectra and the heterogeneous emission of alcohol dehydrogenase. *Biochemistry.* 21:4671–4769.
4. Isenberg, I. 1983. Robust estimation in pulse fluorometry, a study of the method of moments and least squares. *Biophys. J.* 43:141–148.
5. Eisenfeld, J., and C. C. Ford. 1979. A systems-theory approach to the analysis of multiexponential fluorescence decay. *Biophys. J.* 26:73–84.
6. Laws, W. R., and L. Brand. 1979. Analysis of two-state excited-state reactions. The fluorescence decay of 2-naphthol. *J. Phys. Chem.* 83:95–802.
7. Lakowicz, J. R., and A. Balter. 1982. Differential-wavelength deconvolution of time-resolved fluorescence intensities: a new method for the analysis of excited state processor. *Biophys. Chem.* 16:223–240.
8. Hui, M. H., and W. R. Ware. 1976. Exciplex photocopies V. The kinetics of fluorescence quenching of anthracene by *N,N*-dimethylaniline in cyclohexane. *J. Am. Chem. Soc.* 98:4718–4727.
9. Koyava, V. T., V. S. Pavlovich, L. G. Pikulik, and A. M. Sarzhevskii. 1981. *Opt. Spectrosc. (USSR).* 49:159–163.
10. Haas, E., E. J. Katchalski-Katzir, and I. Z. Steinberg. 1978. Brownian motion of the ends of oligopeptide chains in solution as estimated by energy transfer between chain ends. *Biopolymers.* 73:11–31.
11. Fung, B. K. K., and L. Stryer. 1978. Surface density determination in membranes by fluorescence energy transfer. *Biochemistry.* 17:5241–5248.
12. Ware, W. R., S. K. Lee, G. J. Brant, and P. P. Chow. 1970. Nanosecond time-resolved emission spectroscopy: spectral shifts due to solvent-excited solute relaxation. *J. Chem. Phys.* 54:4729–4737.
13. DeToma, R. P., J. H. Easter, and L. Brand. 1976. Dynamic interactions of fluorescence probes with the solvent environment. *J. Am. Chem. Soc.* 98:5001–5007.
14. Badea, M. G., R. P. DeToma, and L. Brand. 1978. Nanosecond relaxation processes in liposomes. *Biophys. J.* 24:197–212.
15. Gafni, A., R. P. DeToma, R. E. Manrow, and L. Brand. 1977. Nanosecond decay studies of a fluorescence probe bound to apomyoglobin. *Biophys. J.* 17:155–168.
16. Ross, J. A., C. J. Schmidt, and L. Brand. 1981. Time-resolved fluorescence of the two tryptophans in horse liver alcohol dehydrogenase. *Biochemistry.* 20:4369–4377.
17. Privat, J. P., P. Wahl, J. C. Auchet, and R. H. Pain. 1980. Time-resolved spectroscopy of trytophyl fluorescence of yeast 3-phosphoglycerate kinase. *Biophys. Chem.* 11:239–248.
18. Spencer, R. D., and G. Weber. 1969. Measurement of subnanosecond fluorescence lifetimes with a cross-correlation phase fluorometer. *Ann. NY Acad. Sci.* 158:361–376.
19. Gaviola, Z. 1926. Ein Fluorometer. Apparat zur Messung von Fluoreszenzabklingungszeiten. *Z. Phys.* 42:853–861.
20. Birks, J. B., and D. J. Dyson. 1961. Phase and modulation fluorometer. *J. Sci. Instrum.* 38:282–385.
21. Bailey, E. A., and G. K. Rollefson. 1953. The determination of the fluorescence lifetimes of dissolved substances by a phase shift method. *J. Chem. Phys.* 21:1315–1326.
22. Van Hock, A., J. Vervoort, and A. J. W. G. Visser. 1983. A subnanosecond resolving spectrofluorometer for the analysis of protein fluorescence kinetics. *J. Biochem. Biophys. Methods.* 7:243–254.
23. Alfono, R. F., editor. 1982. Biological Events Probed by Ultrafast Laser Spectroscopy. Academic Press, Inc., New York. 443 pp.
24. Weber, G. 1981. Resolution of the fluorescence lifetimes in a heterogeneous system by phase and modulation measurements. *J. Phys. Chem.* 85:949–953.
25. Lakowicz, J. R., and H. Cherek. 1981. Phase-sensitive fluorescence spectroscopy. A new method to resolve fluorescence lifetimes or emission spectra of-components in a mixture of fluorophores. *J. Biochem. Biophys. Methods.* 5:19–35.
26. Lakowicz, J. R., and A. Balter. 1982. Direct recording of the initially excited and the solvent relaxed fluorescence of tryptophan by phase sensitive detection of fluorescence. *Photochem. Photobiol.* 36:125–132.
27. Gratton, E., and M. Limkeman. 1983. A continuously variable frequency cross-correlation phase fluorometer with picosecond resolution. *Biophys. J.* 44:315–324.
28. Hauser, M., and G. Heidt. 1975. Phase fluorometer with a continuously variable frequency. *Rev. Sci. Instrum.* 46:470–471.
29. Gratton, E., J. R. Lakowicz, B. P. Maliwal, H. Cherek, G. Laczko, and M. H. Limkeman. 1984. Resolution of mixtures of fluorophores using variable-frequency phase and modulation data. *Biophys. J.* 46:479–486.
30. Kaminov, I. 1974. An Introduction to Electrooptic Devices. Academic Press, Inc., New York. 409 pp.
31. Adhav, S. R., R. S. Adhav, and H. von de Vaart. 1981. Traveling wave amplitude modulator with a 1-GHz bandwidth for coherent light optical communication. *Appl. Opt.* 20:867–871. 336 pp.
32. Gratton, E., and R. Lopez-Delgado. 1980. Measuring fluorescence decay times by phase-shift and modulation using the high harmonic content of pulsed light sources. *Nuovo Cimento B.* 56:110–124.
33. Bevington, P. R. 1969. Data Reduction and Error Analysis for the Physical Sciences. McGraw-Hill, Inc., New York. 336 pp.
34. Marquardt, D. W. 1963. An algorithm for least-square estimation of nonlinear parameter. *J. Soc. Ind. Appl. Math.* 11:431–441.
35. Brandt, S. 1976. Statistical and Computational Methods in Data Analysis. North Holland Publishing Company, Amsterdam, The Netherlands. Second ed. 414 pp.
36. Jameson, D. M., and E. Gratton. 1983. Analysis of the heterogeneous emission by multifrequency phase and modulation fluorometry. *In* New Direction in Molecular Luminesce. D. Eastwood, editor. *Am. Soc. Test. and Mater., ASTM Special Technical Publication.* 822:67–81.
37. Weber, G. 1977. Theory of differential phase fluorometry: detection of anisotropic molecular motions. *J. Chem. Phys.* 66:4081–4091.
38. Solodovnikov, V. V. 1960. Introduction to the statistical dynamics of automatic control systems. Dover Publications, Inc., Mineola, New York. 305 pp.

39. Grinvald, A., and I. Z. Steinberg. 1974. On the analysis of fluorescence decay kinetics by the method of least-squares. *Anal. Biochem.* 59:583–598.
40. Beechem, J., J. R. Knutson, and L. Brand. 1983. Stimulatanous analysis of multiple fluorescence decay curves: a global approach. *Photochem. Photobiol.* 37:S20.
41. Bennet, R. G. 1964. Instrument to measure lifetimes in the micromillisecond region. *J. Chem. Phys.* 41:3037–3041.
42. Bakhshiev, N. G., Y. T. Mazurenko, and I. V. Peterskaya. 1966. Luminescence decay in different portions of the luminscence spectrum of molecules in viscous solution. *Opt. Spectrosc. (USSR).* 21:307–309.
43. Veselova, T. V., L. A. Limareva, and A. S. Cherkasov. 1965. Fluorometric study of the effect of solvent on the fluorescence spectrum of 3-amino-*N*-methylphthalimide. *Opt. Spectrosc. (USSR).* 19:39–43.
44. Ware, W. R., and T. L. Nemzek. 1973. The direct observation of transient effects in diffusion-controlled fluorescence quenching. *Chem. Phys. Lett.* 23:557–560.
45. Lakowicz, J. R., H. Cherek, B. P. Malinial, G. Laczko, and E. Gratton. 1984. Determination of time-resolved emission spectra and anisotropies of a fluorophore-protein complex using frequency-domain phase-modulation fluorometry. *J. Biol. Chem.* In press.